CEIG - Spanish Computer Graphics Conference (2022)
J. Posada and A. Serrano (Editors)

Cylindrical Transform Slicing of Revolute Parts with Overhangs for Laser Metal Deposition

D. Montoya-Zapata[1,2], A. Moreno[1], I. Ortiz[3], O. Ruiz-Salguero[2] and J. Posada[1]

[1]Vicomtech Foundation, Basque Research and Technology Alliance (BRTA), Mikeletegi 57, Donostia-San Sebastian 20009, Spain
[2]Laboratory of CAD CAM CAE, Universidad EAFIT, Cra 49 no 7-sur-50, Medellín 050022, Colombia
[3]Ikergune A.I.E., San Antolin 3, Elgoibar 20870, Spain

Abstract

In the context of Laser Metal Deposition (LMD), temporary support structures are needed to manufacture overhanging features. In order to limit the need for supports, multi-axis machines intervene in the deposition by sequentially repositioning the part. Under multi-axis rotations and translations, slicing and toolpath generation represent significant challenges. Slicing has been partially addressed by authors in multi-axis LMD. However, tool-path generation in multi-axis LMD is rarely touched. One of the reasons is that the required slices for LMD may be strongly non-developable. This fact produces a significant mismatch between the tool-path speeds and other parameters in Parametric space vs. actual Euclidean space. For the particular case of developable slices present in workpieces with cylindrical kernel and overhanging neighborhoods, this manuscript presents a methodology for LMD tool path generation. Our algorithm takes advantage of existing cylindrical iso-radial slicing by generating a path in the (κ, z) parameter space and isometrically translating it into the $\mathbb{R}^3$ Euclidean space. The presented approach is advantageous because it allows the path-planning of complex structures by using the methods for conventional 2.5-axis AM. Our computer experiments show that the presented approach can be effectively used in manufacturing industrial/mechanical pieces (e.g., spur gears). Future work includes the generation of the machine g-code for actual LMD equipment.

CCS Concepts

• ***Computing methodologies*** → *Shape modeling; Modeling and simulation;* • ***Applied computing*** → *Computer-aided design;*

1. Introduction

Laser Metal Deposition (LMD) uses the power of a laser beam to melt a jet metal powder and add it to a workpiece. As opposed to other Additive Manufacturing (AM) processes, LMD does not allow the addition of support structures to build overhanging features. To answer this limitation, researchers are developing multi-axis LMD machines. However, 2.5-axis AM process planning does not apply for the multi-axis case.

1.1. Scope

The kernel, K, of a polygon Q is the convex subset of Q from which all the points in the boundary of Q are visible. This manuscript addresses 3D solid geometries B for which there is an axis $L \subset \mathbb{R}^3$ such that all cross-sections of B perpendicular to L: (i) are connected, (ii) have non-null kernel intersecting L, and (iii) have kernel containing a disk of radius $R > 0$ whose center is in L. These facts imply that L is a common rotation axis for the whole workpiece such that the material dispenser radial position and the angular position of the in-process workpiece can be synchronized so the dispenser is able to deliver the material in all points of the instantaneous periphery of the in-process cross-sections without hitting an already built portion of the workpiece.

Workpieces in which all cross-sections in one direction have kernel but there is no intersection of the projections of the kernels may still be manufactured, but an instantaneous mobile pivot point of the rotation axis will be needed (with its direction ray being constant). This requirement demands a multi-axis milling machine instead of a lathe and will not be considered in this manuscript. We also ignore workpieces for which there exists no vector $\mathbf{n} \in \mathbb{R}^3$ such that every workpiece cross-section (normal to $\mathbf{n}$) contains kernel.

2. Literature Review

In multi-axis AM, the 3D solid may be decomposed into a sequence of simpler workpieces, along with the rigid transformations which re-position the growing workpiece in the multi-axis machine. These 3D set partition algorithms use geometrical and optimization heuristics in order to reduce the usage of ancillary support structures. Refs. [WDF*17, REaL05] use 1D simplifica-

DOI: 10.2312/ceig.20221141

tions (skeletons) of the 3D solid to perform the decomposition. The branches in the skeleton define the sub-solids of the decomposition. Ref. [DPC*16] identifies the zones of higher surface curvature to segment the given solid. Refs. [GWYN19, WDF*20] divide the solid with cutting planes. The placement of the cutting planes minimizes the area (or volume) of the overhanging geometry.

Multi-axis AM allows the deposition of non-planar layers. Ref. [DWW*18] discretizes the solid into voxels to compute synchronized 5-axis non-planar toolpaths that considerably reduce the need for support structures. Refs. [SGM21, XLCT19] define scalar fields (geodesic distance [SGM21] and temperature [XLCT19]) over the volume of the 3D solid. The slices correspond to isolevel surfaces of these scalar fields. Ref. [EMSW21] presents support-minimizer slicing LMD method to fabricate gas exhaust manifolds. Refs. [DDK17, ZMFX18] use cylindrical coordinate transforms to perform cylindrical-based slicing for revolute workpieces. The aforementioned publications do not present a discussion on the generation of tool paths.

2.1. Conclusions of the Literature Review

In the existing literature, several approaches aim to reduce the usage of support structures in AM by using multi-axis machines. Refs. [DDK17, ZMFX18] use coordinate transforms to execute the slicing. The toolpath generation for these slicing methods is still an open research question.This manuscript presents a method to efficiently compute the slices and the toolpaths for 3D solids B with a rotation axis that allows radial access to all borders of B cross-sections. The toolpath generation method uses isometric (i.e., distance-preserving) parametrization along with conventional 2.5-axis toolpath generation [MZCO*21, MZRM*21, MZPA*22] algorithms. This article shows that the presented algorithm can be used for the manufacturing of industrial workpieces, such as spur gears.

3. Methodology

Figure 1 shows the procedure used to slice the B-Rep (skin) of the workpiece and to generate the tool paths to materialize the solid slices. The procedure applies to a workpiece having a revolution axis common to all its axial cuts' kernels. For slicing: (i) apply to the B-Rep a cylindrical transform which maps the revolute workpiece into a prismatic one (in the cylindrical coordinate system). (ii) slice with planes (in the cylindrical coordinate system) the prismatic B-Rep. For tool path generation in each iso-radial flat slice: (a) correct for length warping by computing (in this case) linear re-parametrization particular to each iso-radial slice, (b) apply the algorithms for flat slice tool-path planning, and (c) map tool paths in the cylindrical coordinate system back to Euclidean space iso-radial slices.

3.1. Cylindrical-Based Slicing for Overhanging Geometry

The map from cylindrical $(\theta \in (-\pi, \pi], \rho > 0, z)$ to Cartesian coordinates (x, y, z) is given by:

$$f(\theta, \rho, z) = (x, y, z) = (\rho\cos(\theta), \rho\sin(\theta), z) \tag{1}$$

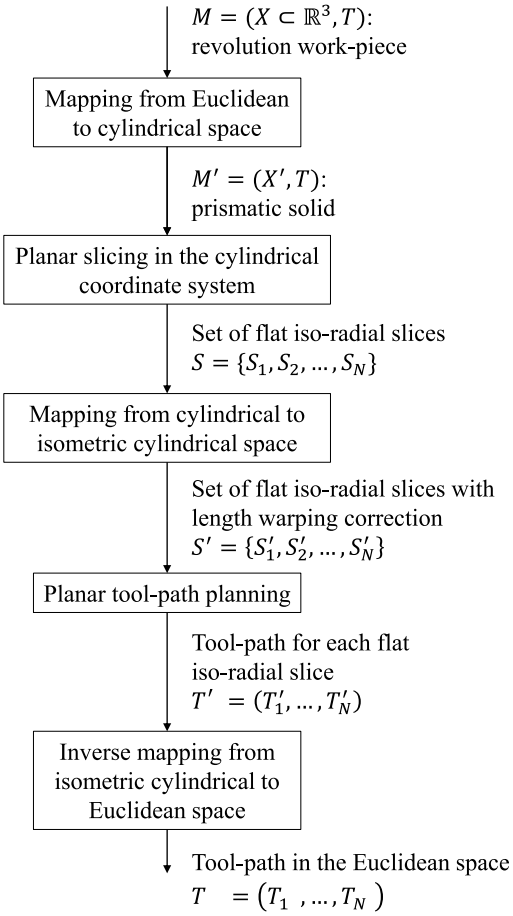

Figure 1: *Workflow for the slicing and toolpath generation.*

The map from Cartesian to cylindrical coordinates is given by:

$$g(x, y, z) = (\theta, \rho, z) = \left(\text{atan2}(y, x), \sqrt{x^2 + y^2}, z\right); \tag{2}$$

$$\text{atan2}(y, x) = \begin{cases} \arccos(x/\rho); & y \geq 0 \\ -\arccos(x/\rho); & y < 0 \end{cases} \tag{3}$$

The representation of a cylinder of radius R, C_R, in Cartesian coordinates is:

$$C_R = \left\{(x, y, z) : x^2 + y^2 = R^2\right\}; \tag{4}$$

which in cylindrical coordinates is the plane:

$$C_R = \{(\theta, \rho, z) : \rho = R\}. \tag{5}$$

Therefore, a slice $\rho = R$ of the prismatic B-Rep in cylindrical coordinates amounts to a cylindrical slice in Cartesian coordinates.

3.2. Toolpath Generation Using Isometric Parametrization

The distance on a plane in cylindrical coordinates does not match the distance on a cylinder in Cartesian coordinates. Therefore, we transform the iso-radial slices in cylindrical coordinates onto the

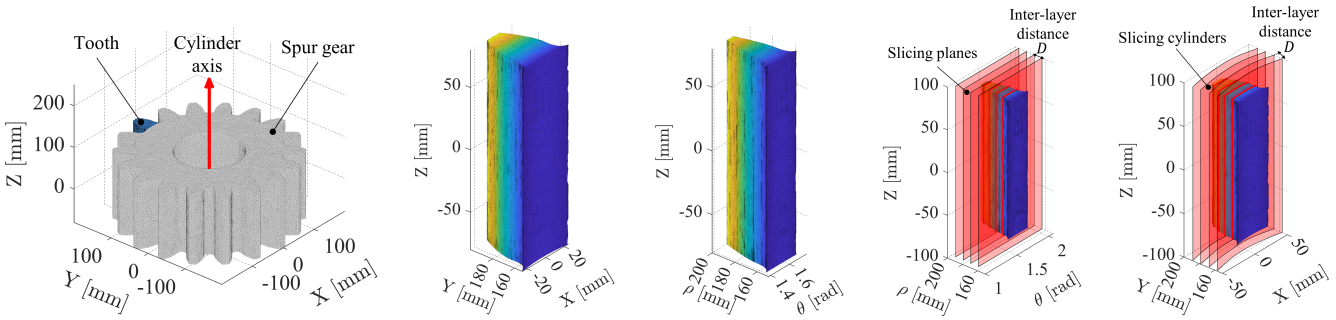

(a) Dataset. Spur gear.

(b) Gear tooth to be manufactured.

(c) Gear tooth in cylindrical coordinates.

(d) Planar slicing in cylindrical coordinates.

(e) Corresponding slicing in Cartesian coordinates.

Figure 2: *Cylindrical-based slicing using coordinate transformation and planar slicing.*

space (κ, R_i, z) which is isometric (i.e., distance-preserving) to the Euclidean space.

Given the slice S_i, which represents the intersection with the plane $\rho = R_i$ in cylindrical coordinates, we apply the following transformation to S_i, $w : S_i \to M_i \subset \mathbb{R}^3$, where M_i is a plane:

$$w(\theta, R_i, z) = (R_i\theta, R_i, z); \quad w^{-1}(\kappa, R_i, z) = (\kappa/R_i, R_i, z). \tag{6}$$

This transformation *stretches* the θ-coordinate as given by the cylinder radius R_i. The map from coordinate (κ, z) to Cartesian coordinates is $h = f \circ w^{-1}$:

$$\begin{aligned} h(\kappa, R_i, z) &= f(w^{-1}(\kappa, R_i, z)) && (7)\\ &= f(\kappa/R_i, R_i, z) && (8)\\ &= (R_i\cos(\kappa/R_i), R_i\sin(\kappa/R_i), z). && (9) \end{aligned}$$

Notice h maps planes in the coordinate system (κ, R_i, z) to cylinders of radius R_i in Cartesian coordinates (x, y, z). The magnitude κ is the arc length measured on the cylinder surface.

Now, we show that the function h is an isometry (i.e., distance-preserving) and a bijection from planes onto cylinders. Let B_1 be the plane defined by the equation $y = R$. Consider the parametrization σ_1 for B_1:

$$\sigma_1(u, v) = (u, R, v) \tag{10}$$

Let B_2 be a cylinder of radius R centered at the origin with parametrization σ_2:

$$\sigma_2(u, v) = (R\cos(u/R), R\sin(u/R), v) \tag{11}$$

Consider the function $h : B_1 \to B_2$:

$$h(x, R, z) = (R\cos(x/R), R\sin(x/R), z) \tag{12}$$

(i) $\sigma_2(u, v) = h(\sigma_1(u, v))$ and (ii) $I_1 = I_2$, where I_i is the first fundamental form of B_i. Therefore, h is an isometry.

(ii) follows from:

$$J_1 = \begin{bmatrix} 1 & 0 \\ 0 & 1 \\ 0 & 0 \end{bmatrix} \quad J_2 = \begin{bmatrix} -\sin(u/R) & 0 \\ \cos(u/R) & 0 \\ 0 & 1 \end{bmatrix}; \quad I_i = J_i^T J_i \tag{13}$$

$$I_1 = \begin{bmatrix} 1 & 0 \\ 0 & 1 \end{bmatrix} = I_2 \tag{14}$$

where J_1 and J_2 are the Jacobians of B_1 and B_2, respectively.

Notice that we apply the same map h to the whole slice S_i in cylindrical coordinates, that is, no local mapping is necessary for each planar patch on S_i.

For all revolution workpieces, the approach in this manuscript cannot be applied when the rotation radius of the deposition spot nears zero. This limitation includes (but is not limited to) cylindrical and conical workpieces. In order to apply our approach, it is necessary to previously build, using traditional additive manufacturing, a cylindrical cob with a minimal finite radius. After this cob is available, our method may proceed. Notice that for cones, there is no finite radius different from 0 at the apex. This would be a theoretical limitation of our proposition. However, conical pieces with a sharp apex are discouraged at the level of mechanical or product design. It is common to introduce a bevel or spherical smoothing at the cone apex.

4. Results

To demonstrate the potential of our approach to manufacture industrial workpieces, we apply our method to the LMD path-planning of one tooth of a spur gear.

Fig. 2(a) displays the geometry of the spur gear that we use for demonstration. Fig. 2(b) shows the tooth to which we apply our slicing and tool-path planning its manufacturing via LMD.

Fig. 2(c) shows the prismatic solid associated to the gear tooth in cylindrical coordinates. We apply conventional planar slicing over this prismatic solid in cylindrical coordinates.

Fig. 2(d) displays the flat slices resulting from the planar slicing. We map the flat slices back to Cartesian coordinates using Eq. 1 to show that each flat slice in cylindrical coordinates corresponds to a cylindrical slice in Cartesian coordinates.

Fig. 2(e) shows the cylindrical slices in Cartesian coordinates.

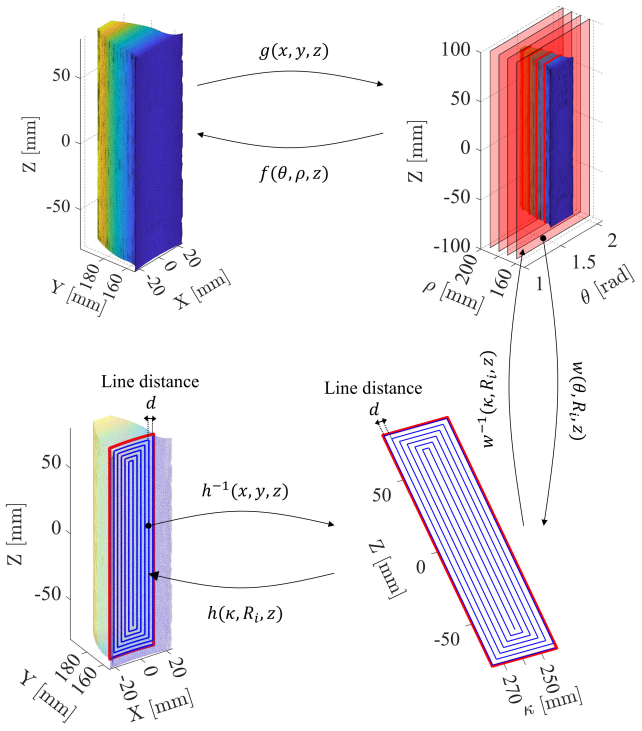

Figure 3: *Toolpath for cylindrical slice using isometric parametrization.*

The distance D between the flat slices in Fig. 2(d) is the same as the distance between the cylindrical slices in Fig. 2(e).

Fig. 3 presents the tool-path generation for *one* of the slices obtained at the previous stage. We use the function w (Eq. 6) to map the flat slices obtained in cylindrical coordinates onto planar patches isometric to cylindrical patches in Cartesian coordinates. We use the spiral infill pattern for the tool-path planning, although other 2D infill patterns may be used. Finally, we map the obtained tool-path onto the cylinder surface in Cartesian coordinates using the function h (Eq. 9).

It is important to remark that the function h preserves the distance d between deposition lines. It is relevant because it allows the tool-path generation on a 2D planar polygonal region (where robust path planning algorithms already exist) instead of on a 3D curved surface. The reader may also notice that one must apply a different transformation to each slice since the function w depends on the cylinder radius R.

As stated in Section 3, our method is suitable for a particular set of revolute workpieces with a cylindrical 3D core. In addition, to meet the condition of self-support, the sub-solids adhered to the cylindrical kernel cannot have prominent overhang features in the radial direction.

5. Conclusions

This manuscript presents a process planning method for Laser Metal Deposition (LMD) of revolute parts. These parts consist of a 3D (informally called *cylindrical*) kernel with overhanging features. Our method maps the B-Rep of the revolute workpiece to cylindrical coordinate space, producing a prismatic B-rep. This prismatic shape is sliced and its slices processed for LMD using 2D path planing tools. The tool paths are corrected for constant velocity and mapped back to Euclidean space thus producing the revolute part. This method is successful for generation of LMD tool paths for spur gear teeth. Future work addresses the actual gear manufacturing.

Funding

This work has been partially funded by the Basque Government under ELKARTEK program (grants KK–2018/00115 (ADDISEND) and KK–2018/00071 (LANGILEOK)), and by the INZU Group (Talens Systems and Ikergune A.I.E.).

References

[DDK17] DING Y., DWIVEDI R., KOVACEVIC R.: Process planning for 8-axis robotized laser-based direct metal deposition system: A case on building revolved part. *Robotics and Computer-Integrated Manufacturing 44* (2017), 67–76. doi:10.1016/j.rcim.2016.08.008. 2

[DPC*16] DING D., PAN Z., CUIURI D., LI H., LARKIN N., VAN DUIN S.: Automatic multi-direction slicing algorithms for wire based additive manufacturing. *Robotics and Computer-Integrated Manufacturing 37* (2016), 139–150. doi:doi.org/10.1016/j.rcim.2015.09.002. 2

[DWW*18] DAI C., WANG C. C. L., WU C., LEFEBVRE S., FANG G., LIU Y.-J.: Support-free volume printing by multi-axis motion. *ACM Trans. Graph. 37*, 4 (2018), 134. doi:10.1145/3197517.3201342. 2

[EMSW21] EISENBARTH D., MENICHELLI A., SOFFEL F., WEGENER K.: Adaptive slicing and process optimization for direct metal deposition to fabricate exhaust manifolds. In *Industrializing Additive Manufacturing* (Cham, 2021), Meboldt M., Klahn C., (Eds.), Springer International Publishing, pp. 160–173. doi:10.1007/978-3-030-54334-1_12. 2

[GWYN19] GAO Y., WU L., YAN D.-M., NAN L.: Near support-free multi-directional 3D printing via global-optimal decomposition. *Graphical Models 104* (2019), 101034. doi:10.1016/j.gmod.2019.101034. 2

[MZCO*21] MONTOYA-ZAPATA D., CREUS C., ORTIZ I., ALVAREZ P., MORENO A., POSADA J., RUIZ-SALGUERO O.: Generation of 2.5D deposition strategies for LMD-based additive manufacturing. *Procedia Computer Science 180* (2021), 280–289. doi:10.1016/j.procs.2021.01.165. 2

[MZPA*22] MONTOYA-ZAPATA D., POSADA J., ALVAREZ P., CREUS C., MORENO A., ORTIZ I., RUIZ-SALGUERO O.: Experimental and computational assessment of minimizing overfill in trajectory corners by laser velocity control of laser cladding. *The International Journal of Advanced Manufacturing Technology* (2022). doi:10.1007/s00170-021-08641-8. 2

[MZRM*21] MONTOYA-ZAPATA D., RODRÍGUEZ J. M., MORENO A., RUIZ-SALGUERO O., POSADA J.: Nonlinear thermal simulation of laser metal deposition. *Australian Journal of Mechanical Engineering 19*, 5 (2021), 653–668. doi:10.1080/14484846.2021.1988435. 2

[REaL05] RUAN J., EIAMSA-ARD K., LIOU F. W.: Automatic multi-axis slicing based on centroidal axis computation. In *International Design Engineering Technical Conferences and Computers and Information in Engineering Conference. Volume 3: 25th Computers and Information in Engineering Conference, Parts A and B* (Long Beach, CA, USA, 2005), pp. 383–393. doi:10.1115/DETC2005-85261. 1

[SGM21] SHAN Y., GAN D., MAO H.: Curved layer slicing based on isothermal surface. *Procedia Manufacturing 53* (2021), 484–491. doi:10.1016/j.promfg.2021.06.081. 2

[WDF*17] WU C., DAI C., FANG G., LIU Y.-J., WANG C. C.: RoboFDM: A robotic system for support-free fabrication using FDM. In *2017 IEEE International Conference on Robotics and Automation (ICRA)* (2017), pp. 1175–1180. doi:10.1109/ICRA.2017.7989140. 1

[WDF*20] WU C., DAI C., FANG G., LIU Y.-J., WANG C. C. L.: General support-effective decomposition for multi-directional 3-D printing. *IEEE Transactions on Automation Science and Engineering 17*, 2 (2020), 599–610. doi:10.1109/TASE.2019.2938219. 2

[XLCT19] XU K., LI Y., CHEN L., TANG K.: Curved layer based process planning for multi-axis volume printing of freeform parts. *Computer-Aided Design 114* (2019), 51–63. doi:10.1016/j.cad.2019.05.007. 2

[ZMFX18] ZHAO G., MA G., FENG J., XIAO W.: Nonplanar slicing and path generation methods for robotic additive manufacturing. *The International Journal of Advanced Manufacturing Technology 96*, 9-12 (2018), 3149–3159. doi:10.1007/s00170-018-1772-9. 2